

RESEARCH

Open Access



Optimized zymogram protocol from 3D spheroid cultures to study MMP-2 and -9 activities in tumor cells

Sandra Majo^{1†}, Chloe Redoute-Timonnier^{1†} , Aurelie Lacour¹, Laurine Challeat¹, Eva Epinette¹, Jeremie Teillon², Christophe F. Grosset¹  and Patrick Auguste^{1*} 

Abstract

Three-dimensional spheroids are more representative of tumors than cell-cultured monolayers. As in tumors, gradients of oxygen, nutrients and wastes are found in spheroid cultures but not in classical cultured monolayers. On the other hand, cell-based assays on the latter are hardly applicable to spheroid cultures. Such is the case for zymogram assays, which are classically used to measure MMP-2 and MMP-9 activities, and for immunoblots to measure the phosphorylation of proteins involved in ligand-induced intracellular signaling in normal and tumor cells. In this study we used two renal cancer cell lines as models, the first derived from a pediatric rhabdoid tumor and the second from an adult clear cell renal cell carcinoma. Using these two cell lines, we successfully developed a simple inexpensive assay to measure MMP-2 and MMP-9 activities in spheroids established in the presence of methylcellulose. After washing, 1 to 5 spheroids were pooled and stimulated with collagen I for 24 h before analysis. MMP-2 and MMP-9 activities were measured in supernatants using a standard but enhanced zymogram assay. Both pro-MMP-9 and MMP-2 activities were detected in spheroids established from both cell lines. In contrast with our previous data using classical cultures monolayers, collagen I stimulation decreased pro-MMP-9 activity without affecting MMP-2 activity. On the other hand, we could not accurately measure AKT intracellular signaling pathways from spheroids stimulated with collagen I. Finally, we adapted our 3D protocol to analyze the MAPK/ERK pathway in kidney tumor cells following induction by EGF. In conclusion, this zymogram assay for analyzing MMP-2 and MMP-9 activities in spheroids paves the way for novel experimentations in tumor biology.

Keywords Renal cancer cells, 3D tumor model, Spheroid, Collagen I, MMP-2, MMP-9, Zymogram assay, AKT pathway, ERK pathway

[†]Sandra Majo and Chloe Redoute-Timonnier contributed equally to this work.

*Correspondence:

Patrick Auguste

patrick.auguste@inserm.fr

¹Univ. Bordeaux, INSERM, BRIC, U1312, MIRCADE team, Bordeaux F-33000, France

²Univ. Bordeaux, CNRS, INSERM, BIC, USA, UAR 3420, Bordeaux F-33000, France



Introduction

Most studies using tumor cell lines are performed with cell-cultured monolayers on plastic dishes. In 2D cultures, all cells are grown in high, uniformly distributed O₂ concentrations in contact with sufficient nutrients, growth factors and other soluble factors. Moreover, plastic influences the gene program, cell state and differentiation [1]. These conditions are far removed from those found in real tumors, in which cells grow, develop, and evolve in 3D. Cells grow in tumors in the presence of a gradient concentration of oxygen undergoing hypoxic activation of the HIF signaling pathway and secretion of hypoxia-inducible factors such as VEGF [2]. Moreover, metabolite and waste concentrations vary within tumors [3]. Tumor cells interact closely and communicate with the surrounding microenvironment which is comprised of stromal cells and the extracellular matrix (ECM) [3–5]. Spheroids are 3D tumor cell structures mimicking some of the bio-architectural characteristics found in tumor tissues. Spheroids with a diameter of 200 µm or more display a metabolic and waste gradient as in tumors, and those with a diameter of 500 µm or more have a hypoxic center [1, 6].

To metastasize, tumor cells acquire a mesenchymal phenotype, cleave basement membrane and interstitial ECMs, migrate, intravasate and extravasate blood or lymphatic vessels [7]. Proteolysis of the ECM is crucial for metastasis to occur. Its degradation is mediated by various enzymes, including matrix metalloproteinases (MMP). The MMPs belong to a family of 26 zinc activated enzymes and are organized as transmembrane proteins, glycosylphosphatidylinositol (GPI) anchored proteins or secreted proteins [7, 8].

MMP-2 and small - (as MMP-2): -9 belong to the gelatinase subfamily of MMPs. They are first synthesized as inactive pro-MMPs by tumor and stromal cells, the pro-peptide domain inactivating the catalytic domain. Once secreted, the pro-peptide domain is cleaved by various proteases and the activated enzymes can then degrade denatured collagen (gelatin) and a wide range of ECM proteins and proteoglycans [7, 8].

In vitro, MMP-2 and small - (as MMP-2): -9 activities are routinely measured with an assay called zymogram where non-boiled samples are loaded into a non-reducing SDS PAGE containing gelatin. Following gel migration, MMP-2 and small - (as MMP-2): -9 are renatured and activated, allowing the degradation of gelatin around their migratory position. The location of activated MMP-2 and small - (as MMP-2): -9 proteins in gel after migration is revealed by Coomassie-blue staining, and digested gelatin appears as clear bands on a blue gel background. This simple effective method allows the detection of both pro- and activated MMP-2 and small - (as MMP-2): -9 activities with molecular weights of 92

and 82 kDa for pro- and MMP-9, and 72 and 62–64 kDa for pro- and MMP-2, respectively [9].

Kidney cancers account for 3–5% of all cancers occurring in children and adults. There are several subtypes, the most common form being Wilms tumor in children [10] and clear cell Renal Cell Carcinoma (ccRCC) in adults [11]. In children, the rare Rhabdoid Tumor of the Kidney (RTK) has the worst 5-year overall survival, which is only 15% for stage III-V. It is associated with loss of function of the SMARCB1 gene coding for a subunit of the chromatin remodeling complex SWI/SNF [10]. In adults, ccRCC represents around 75% of all kidney tumors, of which 70–80% harbor an inactivation of the tumor suppressor gene VHL. Moreover, 35% of ccRCC patients at diagnosis and 20–40% of patients after nephrectomy develop metastases. However, 5-year overall survival is satisfactory and reaches 47 months [11, 12].

We established spheroids deriving from two different kidney cancer cell lines and studied extracellular MMP-2 and Small - (as MMP-9): -9 activities in cell supernatants. We designed a protocol including prolonged stimulation of spheroids with collagen I and a zymogram assay to investigate pro- and activated MMP-2 and Small - (as MMP-9): -9 functioning. The same cultured protocol was used to analyze the AKT intracellular pathway following tumor cell activation by collagen I. Finally, we adapted our 3D protocol to study the MAPK/ERK pathway in kidney tumor cells.

Materials & methods

Cell culture

The human cell lines WT-CLS1 and 786-O were used. WT-CLS1 cells, which were derived from a pediatric RTK, were obtained from the CLS company (Cell Lines Service (Cytion), Germany). The adult ccRCC 786-O cell line was a gift from Pr A. Bikfalvi (BRIC, U1312, Bordeaux, France). Both cell lines were cultured in complete medium composed of RPMI 1640 medium with Gluta-MAX™ (Gibco, ref#61870-010) supplemented with 10% fetal bovine serum (FBS, PAN Biotech, ref#30-3306) and 1% penicillin-streptomycin (Gibco, ref#15070-063) at 37 °C and 5% CO₂. Cell authenticity was certified by the Eurofins - Cell Line Authentication service and cells were tested weekly for the absence of mycoplasma.

Spheroid formation

For both cell lines, spheroids were formed in a U-bottom 96-well plate not treated for cell culture (Starstedt ref#83.3925500) using 1% methylcellulose (Sigma-Aldrich, ref#M7027) prepared in phosphate buffer saline (PBS). For one spheroid, 10,000 cells in 50 µl of complete medium were mixed with 50 µl of 1% methylcellulose and deposited in a well of the U-bottom 96-well plate. After incubation for 3 days at 37 °C and 5% CO₂, cells

spontaneously formed spheroids. In some conditions, spheroids were formed in the presence of 100 µg/ml of collagen I (Corning ref#354236), as described above.

Spheroid stimulation with collagen I

ClearLine® microtubes (Dutscher, ref# 390903) were used to monitor spheroids with a microscope throughout the protocol. Spheroids were washed in PBS to remove the methylcellulose. One to 5 spheroids were gently collected from the U-bottom microplate using a pipette with wide-orifice tips (Dutscher, ref#077157) and transferred to a microtube containing 1 ml of PBS. The correct spheroid number per tube and spheroid integrity were checked with a microscope. After removing PBS with a 1 ml pipette and verifying the spheroid number and integrity, 50 µl of RPMI 1640 medium (with GlutaMAX™ but without FBS or penicillin-streptomycin) containing collagen I or not at a final concentration of 100 µg/ml were added to each microtube. Spheroids were incubated for 24 h at 37 °C and 5% CO₂ on a shaker at 30 rpm (N-BIOTEK, ref#NB-T101SRC).

For microscopic analyses, one or five washed spheroids were incubated inside wells of an ultralow absorption 96 well plate (Corning®, ref#3474) and incubated as described above.

Sample preparation for zymogram and western blot

After incubation, the microtubes containing the spheroids were centrifuged at room temperature and at 14,000 rpm for 5 min. For the zymogram assay, 20 µl of spheroid supernatant were collected and mixed with 5 µl of 5X Laemmli loading buffer (250 mM Tris-Cl pH 6.8, 50% Glycerol, 10% SDS, 0.5% Bromophenol blue) without reducing agent. Samples were not boiled before loading on gel. For intracellular cell signaling analysis by western blot, the remainder of the spheroid supernatant was eliminated (approximately 30–35 µl, until the spheroids were mostly dry) and 25 µl of 1X Laemmli loading buffer containing 2% β-mercaptoethanol (Sigma-Aldrich, ref#M3148) were added. Samples were vigorously vortexed, heated for 5 min at 95 °C and sonicated for 3 s to break the DNA.

Zymogram gel

A 10% polyacrylamide gel containing 0.1% porcine gelatin (Sigma-Aldrich, ref#G1890) was prepared. After polymerization, the 5% polyacrylamide gel was added. After loading the samples and protein ladder, migration was performed for 90–120 min at 100 volts in a regular Tris-glycine-SDS buffer (Euromedex, ref#EU0510) until the blue dye ran out of the gel. After migration the gel was washed 4 times for 15 min with a 2.5% Triton X100 (Euromedex, ref#2000) solution. Then, the gel was incubated at 37 °C in a water bath with the developing solution (50 mM Tris HCl pH 7.4,

0.2 M NaCl and 10 mM CaCl₂) for 48 h. Next, the developing solution was removed, and the gel was further incubated at 37 °C for 12–15 h in the same developing solution. The gel was stained with Coomassie blue solution (0.5% Coomassie blue in 50% ethanol and 10% acetic acid) for 15–30 min and washed in 30% acetic acid and 10% ethanol solution until the MMP bands became visible. The gel was stored in distilled water for 3 days at room temperature and the picture was taken using a Chemidoc imaging system (Bio-Rad). The intensity of each band was quantified with Fiji software. Similarities and differences between our 2D [12] and 3D protocols is shown in Supplementary Table 1.

Spheroid images

Confocal microscopy images were acquired using a LEICA TCS SP8 mounted on a DMI6000 inverted stand (Leica Microsystems, Mannheim, Germany) with a 10X NA 0.30 HC Plan Fluotar dry objective. Sample autofluorescence was excited with a pulsed white laser at 520 nm and signals were collected between 570 and 790 nm on an internal photomultiplier tube. Z-stack were acquired with a z-step of 5 µm. In parallel, a bright-field photography of each sample was also acquired.

RNA extraction

RNA extraction was performed using 5 spheroids cultured with or without collagen I in the seeding and/or in the medium (see above for a more detailed protocol). NucleoSpin RNA extraction kit (MACHEREY NAGEL, ref#740955.250) was used according to manufacturer's instructions, except for RNA elution performed with 30 µl of 60 °C DNase/RNase-Free distilled water (Invitrogen, 11538646). Total RNAs were quantified using a spectrophotometer (Trinean).

RT-qPCR

Complementary DNAs (cDNAs) were synthesized with random hexamer primers from 250 ng of total RNA using Maxima Reverse Transcription kit (ThermoFisher Scientific, ref#EP0743) according to manufacturer's instructions. cDNAs were diluted (1/10) in DNase/RNase-Free Distilled Water. Quantitative PCRs were performed in duplicate on a CFX opus 96 (Bio-Rad) thermal cycler using SYBR Green qPCR Master Mix (No ROX) (Med-ChemTronica, #HY-K0523). The cycling parameters included 39 cycles of denaturation at 95 °C for 5 s and annealing-elongation at 60 °C for 30 s. Primers (Eurofins) used to assess the mRNA expression of targeted genes are shown in Table 1. GAPDH and 18S ribosomal RNAs served as internal controls for normalization. At the end of the PCR, a melting curve was obtained by increasing the temperature from 65 to 95 °C.

Table 1 Primers used in qPCR analysis –18S forward –18S reverse

Target	Human sequence
MMP-2 forward	5' GGAGACAAGTTCTGGAGATACAATG 3'
MMP-2 reverse	5' TTTGGTTCTCCAGCTTCAGGTA 3'
MMP-9 forward	5' GTTCCCGGAGTGAGTTGAAC 3'
MMP-9 reverse	5' TTTACATGGCACTGCCAAAGC 3'
GAPDH forward	5' CAAGGAGTAAGACCCCTGGA 3'
GAPDH reverse	5' AGGGGAGATTCAGTGTGGTG 3'
18 S forward	5' GTAACCCGTTGAACCCCAT 3'
18 S reverse	5' CCATCCAATCGGTAGTAGCG 3'

Western blotting

A 10% polyacrylamide gel was prepared. After polymerization, the 5% polyacrylamide gel was added. After loading the sample and protein ladder, migration was performed for 90–120 min at 100 volts in a regular Tris-glycine-SDS buffer until the blue dye ran out of the gel. Proteins were transferred onto a nitrocellulose membrane (Amersham™ Protran, ref#10600011) using a Tris-glycine buffer (Euromedex, EU0550) containing 10% ethanol for 70 min at 100 Volts. The membrane was washed in distilled water and incubated with Ponceau S staining solution (Sigma Aldrich, ref#P7170) for 2 min. After a quick wash in deionized water, a picture of the membrane was taken using a Fusion FX6 imaging system (Vilber Lourmat, Marne-la-Vallée, France). Next, the membrane was blocked in 5% non-fat milk in TBS-T (TBS, Tris Buffer Saline (Euromedex, ref#ET2020) containing 0.1% Tween 20 (Euromedex, ref#2001-C)) for 45 min. Then, the membrane was incubated overnight under agitation at 4 °C with a rabbit anti-phospho-AKT (Ser 473) (p-AKT) antibody (Cell Signaling, ref#9271S) diluted at 1:1000 in TBS-T 5% BSA (Bovine Serum Albumin, PAN Biotech, ref#P06-1391500). The membrane was washed under agitation 5 times for 5 min in TBS-T. A goat anti-rabbit antibody conjugated to a fluorophore (LICOR IRDye800CW, ref#926-32211) diluted at 1:5000 in TBS-T 5% BSA was added. After 1-hour incubation, the membrane was washed under agitation 3 times for 5 min in TBS-T and twice for 5 min in TBS. Fluorescence intensity was measured with a ChemiDoc imaging system. Then, the membrane was incubated overnight at 4 °C under agitation with a mouse anti-AKT antibody (1:1000; Cell Signaling, ref#2920S) in TBS-T 5% BSA. The membrane was washed 5 times for 5 min under agitation in TBS-T and a goat anti-mouse antibody conjugated to horseradish peroxidase (Bio-Rad, ref#1706516) diluted at 1:3000 in TBS-T 5% BSA was added. After 1-hour incubation, the membrane was washed 3 times for 5 min under agitation in TBS-T and twice for 5 min in TBS. AKT signals were revealed with a Clarity™ Western ECL Substrate kit (Bio-Rad, ref#170–5061). A photo of the membrane was taken using the Fusion FX6 imaging

system. AKT and p-AKT signals were quantified using Fiji software, and p-AKT signal was normalized to the intensity of the corresponding AKT signal.

Cell viability

Cell viability was analyzed by the Promega CellTiter-Glo® 3D Cell Viability Assay (Promega, ref#G9682). The spheroids were prepared and stimulated as in the zymogram assay. After 24 h incubation, spheroids and their media were transferred to an opaque walled 96-well microplate. Twenty-five µl of the CellTiter-Glo 3D reagent were added and the microplate was shaken for 5 min at room temperature. It was then incubated at room temperature without shaking for another 45 min before reading with a Clariostar microplate reader (BMG Labtech).

ERK activation analysis

ERK phosphorylation was analyzed in monolayer and spheroid cultures. In monolayer cultures, 80% confluent cell plates were starved in RPMI media for 12 h and stimulated or not with 300 ng/mL of EGF (MedChemExpress, ref#HY-P7109) for 5, 15, 45 or 90 min at 37 °C. After a quick wash in PBS, cells were lysed 15 min at 4 °C using RIPA buffer (Sigma-Aldrich, ref#R0278) and centrifuged at 20,000 g for 15 min. Proteins contained in the supernatant were quantified using Pierce™ BCA Protein Assay Kit (Thermo Scientific, ref#23227). 20 µg of proteins were denatured in Laemmli loading buffer containing β-mercaptoethanol and boiled 5 min at 95 °C. In 3D culture, 5 spheroids were collected, washed, combined and starved in 25 µl of RPMI medium for 12 h as previously described. Then, some spheroids were treated by EGF at a final concentration of 300 ng/mL and further incubated for 5, 15, 45 or 90 min at 37 °C. Control spheroids were left untreated. Finally, treated and control spheroids were pelleted, the supernatant was removed and 25 µl of 1X Laemmli loading buffer containing β-mercaptoethanol were added on each pellet. Samples were vigorously vortexed, heated for 5 min at 95 °C and sonicated for 3 s to break the DNA.

Western blotting was performed as described above, and analyzed with a mouse anti-phospho-ERK1/2 IgG (p-ERK, Phosphorylated p44/42 Thr202 and Tyr204) (1:1000 dilution, Cell Signaling, ref#9106S) and with a goat anti-mouse IgG conjugated to a fluorophore (1:5000; LICOR IRDye800CW, ref#926-32210). After fluorescence analysis with a ChemiDoc imaging system, the membrane was probed with a rabbit anti-ERK1/2 antibody (ERK, p44/42) (1:1000 dilution, Cell Signaling, ref#9102S), then with a goat anti-rabbit IgG conjugated with horseradish peroxidase (1:5000 dilution, Sigma-Aldrich, ref#A0545) and revealed with a Clarity™ Western ECL Substrate kit. A membrane was imaged using the Fusion FX6 imaging system. ERK and p-ERK signals were quantified using Fiji

software. p-ERK signal was normalized to the intensity of the corresponding total ERK signal.

Statistics

Statistical analysis was performed with the GraphPad Prism 8.4.1 software. Two groups of values were compared with the non-parametric Wilcoxon-Mann-Whitney test. More than two groups of values were compared with the non-parametric Kruskal-Wallis test, followed by Dunn's Multiple Comparison Test. Data were considered significant when p-value was <0.05.

Results

To study MMP-2 and -9 activities secreted by adult and pediatric renal cancer cells in 3D conditions, we first formed spheroids using methylcellulose from the two renal cancer cell lines 786-O and WT-CLS1. Spheroids were washed and stimulated with collagen I. Supernatants were used to investigate MMP-2 and -9 activities 24 h later.

Our goal was double: to determine whether the formed spheroids can secrete MMP-2 and -9 and to evaluate the sensitivity of our assay. We first tried to form large spheroids by plating 10,000 to 50,000 cells per well in 0.5% methylcellulose. However, it was challenging to manipulate them without altering their 3D organization and the results were not reproducible (data not shown). We therefore developed another procedure by plating 10,000 cells per well in 0.5% methylcellulose and grew cells for 72 h. The spheroids were collected and gently washed to remove methylcellulose. Then, one to five spheroids were pooled in a microtube containing a small amount (50 μ l) of serum-free medium in the absence or presence of collagen I and were further incubated for 24 h under gently agitation at 37 °C and 5% CO₂. During this period, spheroids incubated with collagen I fused to form a single large 3D structure. In absence of collagen I, the 786-O and WT-CLS1 spheroids started to fuse; however, the fusion was incomplete (Supplementary Fig. 1). Compared to incompletely-fused spheroids growing in absence of matrix, the thickness of the fused spheroids in presence of collagen I was 2 and 2.5 times higher for 786-O and WT-CLS1, respectively. Twenty-four hours later, supernatants were collected and analyzed with a standard but optimized zymogram assay. As shown in Figs. 1, 786-O spheroids expressed both pro-MMP-9 (92 kDa) and active MMP-2 (62 kDa) (Fig. 1A-C), an effect that was independent of collagen I stimulation. As expected, MMP activity increased with the number of spheroids (Fig. 1B-C). However, in the presence of collagen I, MMP-2 activity steadily increased with the number of spheroids, while pro-MMP-9 activity reached a plateau when three or more spheroids were pooled (Fig. 1A-C).

WT-CLS1 spheroids expressed fewer active MMP-2 than 786-O spheroids (data not shown, but Fig. 1A and D were treated similarly) and more pro-MMP-9 activity than MMP-2 activity (Fig. 1D). Independently of collagen I stimulation, pro-MMP-9 activity steadily increased with WT-CLS1 spheroid number (Fig. 1D-F). This effect was less pronounced for MMP-2 activity, likely because of a lower MMP-2 activity in WT-CLS1 spheroids (compare Fig. 1A and D).

Intriguingly, active MMP-9 (82 kDa) and pro-MMP-2 (72 kDa) were not detected in any renal cancer spheroids, unlike in renal cancer cells growing as monolayers where we observed pro- and active MMP-9 (92 and 82 kDa, respectively) and active MMP-2 (62–64 kDa) [12]. These paradoxical data suggest that the expression of the pro and active forms of MMPs depends on the growth conditions. Therefore, the culture modality can cause an experimental bias.

Next, we compared the effect of collagen I on pro-MMP-9 and MMP-2 activities. For each cell line and spheroid number, we normalized the pro-MMP-9 expression or the MMP-2 activity obtained in the absence of collagen I stimulation. For the 786-O cell line, collagen I decreased pro-MMP-9 activity and the effect was particularly visible and reproducible with four and five spheroids (Fig. 2A). In contrast, only a small decrease in MMP-2 activity was observed when five 786-O spheroids were cultured in the presence of collagen I (Fig. 2B). These 3D culture results contrasted with those obtained in 2D culture, where MMP-2 activity was increased after collagen I stimulation [12].

By pooling two to five WT-CLS1 spheroids in culture, a decrease in pro-MMP-9 expression was also observed after stimulation with collagen I (Fig. 2C). Surprisingly, pro-MMP-9 expression increased when only one spheroid was stimulated with collagen I. This may have been due to a low expression (Fig. 1F) and/or a limit in the sensitivity of our assay (Fig. 2C). No clear reproducible variation in MMP-2 activity was observed in WT-CLS1 spheroids, very likely because of its low expression in these cells (Fig. 2D).

The lower pro-MMP-9 protein amount in the presence of collagen I could be due to a negative transcriptional, post-transcriptional, translational and post-translational regulation of the gene in 786-O or WT-CLS1 cells, but also to a decrease in cell viability as a result of collagen I-induced cell death. To test these two hypotheses, we conducted a cell viability assay using the CellTiter-Glo 3D assay (Promega) and one to five spheroids. As shown in Fig. 3A and B, no difference in cell viability was observed with 786-O and WT-CLS1 spheroids grown in the presence of collagen I compared to untreated spheroids.

To determine whether the decrease in pro-MMP-9 and -2 activities in spheroid supernatants was due to a

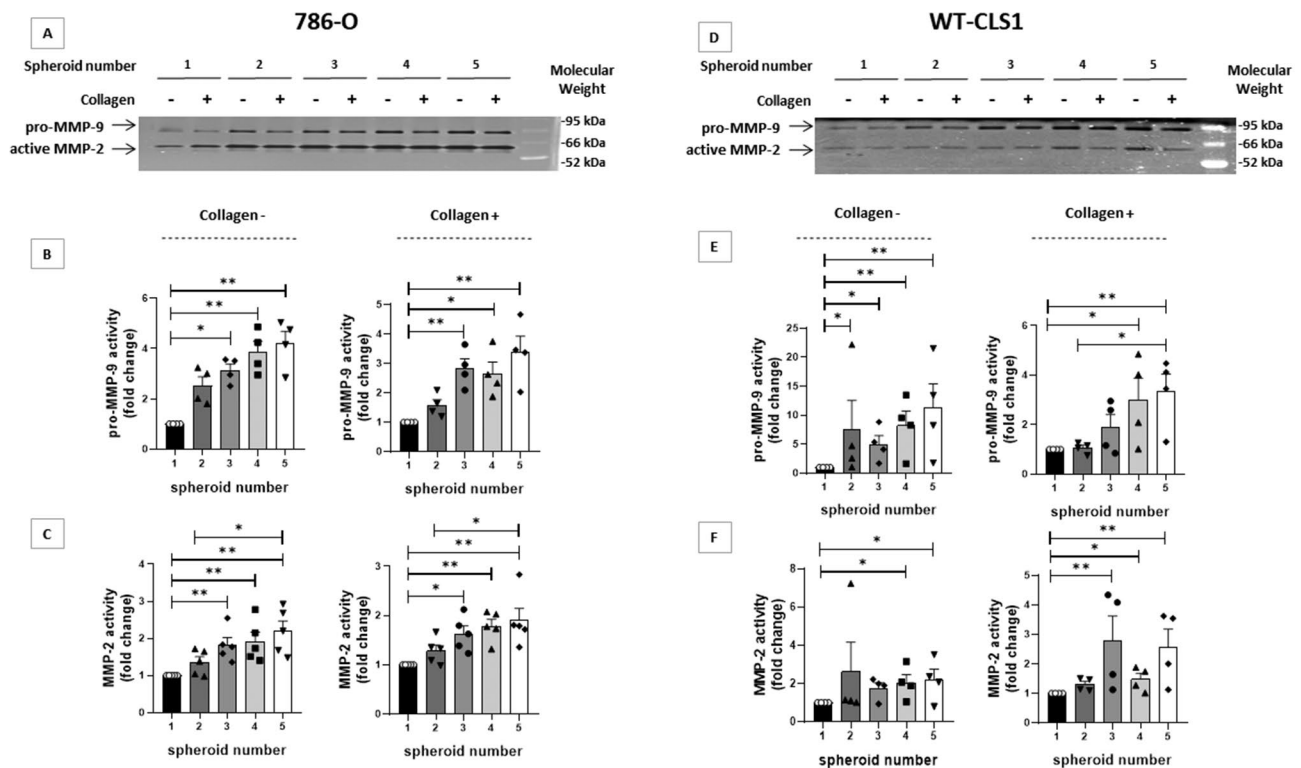


Fig. 1 Zymogram analysis of MMP-2 and -9 activities in the supernatants of kidney cancer spheroid cultures. Representative zymogram assay using 786-O (A) or WT-CLS1 (D) cell growth supernatants. One to five spheroids were pooled before supernatant collection. Pro-MMP-9 is shown as a 92 kDa protein and active MMP-2 as a 62 kDa protein. Activity of pro-MMP-9 in 786-O (B) or WT-CLS1 (E) spheroids cultured in absence (left graph) or presence (right graph) of 100 μ g/ml collagen I. Remark: in absence of collagen I for two spheroids one data out of range increases the mean value. Activity of MMP-2 in 786-O (C) or WT-CLS1 (F) spheroids cultured in absence (left graph) or presence (right graph) of collagen I. Remark: in absence of collagen I for two spheroids one data out of range increases the mean value. For each independent experiment, band intensities were quantified using Fiji software and were normalized to the intensity of a single spheroid band. Data are presented as the mean \pm SEM of 4 to 5 independent experiments ($n=5$ for 786-O and $n=4$ for WT-CLS1 spheroid cultures). * $p < 0.05$ and ** $p < 0.01$, Kruskal-Wallis test, followed by Dunn's Multiple Comparison Test

reduction in MMPs secretion or in transcript abundance into the cells, we measured *MMP2* and *MMP9* mRNA levels in the different spheroid conditions by RT-qPCR. In WT-CLS1 spheroids, *MMP2* and *MMP9* mRNAs were not deregulated by collagen I stimulation (Fig. 4C and D). However, in this cell line, *MMP2* and *MMP9* mRNA levels were very low, at the limit of the qPCR sensitivity, therefore limiting the impact of our data. In 786-O spheroids stimulated with collagen I (Fig. 4A), *MMP9* mRNA increased, while no difference was observed for *MMP2* mRNA (Fig. 4B). Since collagen I increased *MMP9* mRNA abundance and decreased MMP-9 protein secretion, we performed western-blot analysis to determine if collagen I inhibits *MMP9* mRNA translation and/or secretion. Unfortunately, the anti-MMP9 antibody was not sensitive enough to detect pro-MMP-9 and MMP-9 proteins into the cells and in cell supernatants (data not shown).

As a comparison, we treated cells with collagen I (100 μ g/ml) or not for the 72 h required to form spheroids. Thereafter, it was impossible to wash and transfer the WT-CLS1 spheroids to microtubes without

significantly altering their 3D organization. In contrast, with 786-O cells, we were able to obtain and manipulate spheroids like those formed in the absence of collagen I. Interestingly, a zymogram showed an increase in pro-MMP-9 and in MMP-2 activity when spheroids were formed in the presence of collagen I in comparison to spheroids formed without it (Supplementary Fig. 2A and B). Nevertheless, a strong increase in cell viability was observed, suggesting that the increase in MMP-9 and -2 activities when spheroids were formed in the presence of collagen I might not be due to collagen I but rather an increase in cell number (Supplementary Fig. 2C). Thus, we analyzed the *MMP2* and *MMP9* mRNA abundance in 786-O spheroids formed in presence or absence of collagen I. Our data showed that *MMP9* mRNA increases in spheroids formed in presence of collagen I compared to spheroids formed without collagen I. No further increase was observed when collagen I was added in the seeding and in the medium (Supplementary Fig. 2D). In the same experimental conditions, no differences were observed in *MMP2* mRNA abundance (Supplementary Fig. 2E).

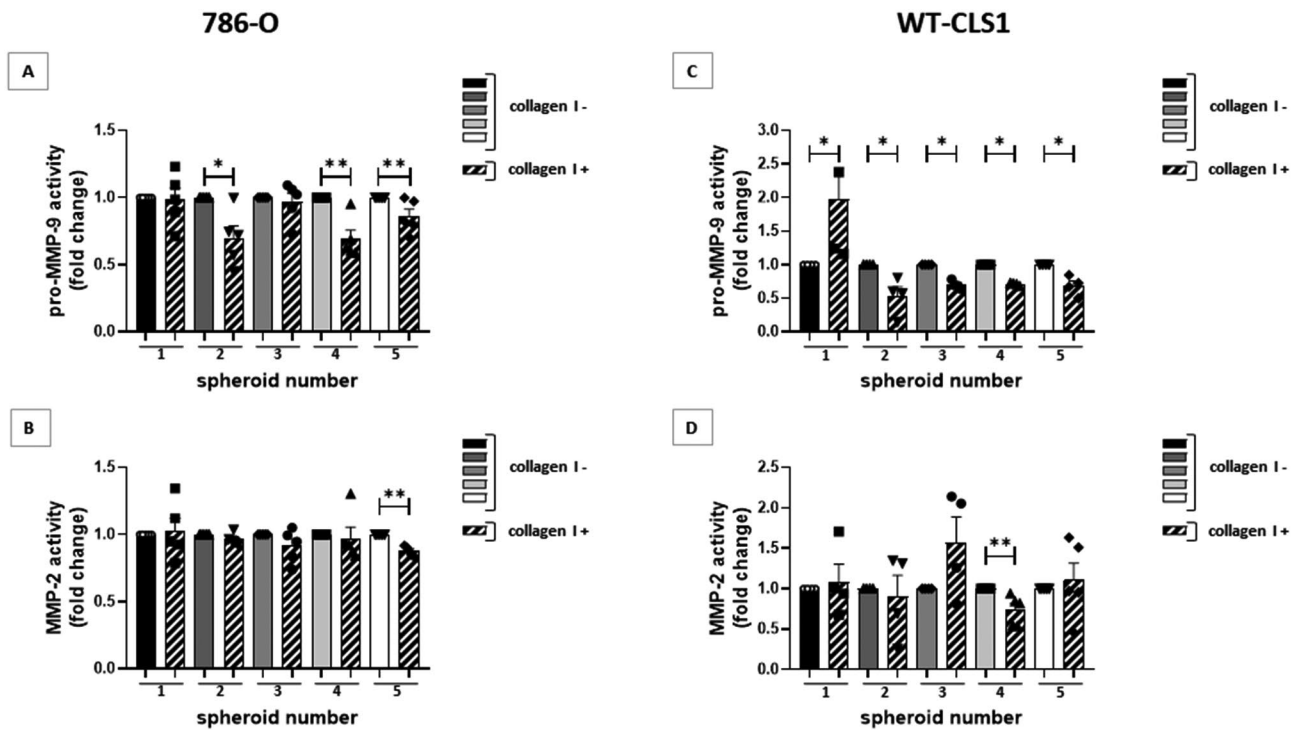


Fig. 2 Effect of collagen I on MMP-2 and -9 activities in supernatant of kidney cancer spheroid cultures. Activities of pro-MMP-9 in 786-O (A) or WT-CLS1 (C) spheroids cultured in absence or presence of collagen I measured in a zymogram assay. Zymogram analysis of MMP-2 activity in 786-O (B) or WT-CLS1 (D) spheroids cultured in absence or presence of collagen I. One to five spheroids were pooled and cultured for 24 h. For each independent experiment, pro-MMP-9 (92 kDa) and active MMP-2 (62 kDa) band intensities were quantified using Fiji software and normalized to the corresponding condition without collagen I. Data are presented as the mean \pm SEM of 4 to 5 independent experiments ($n=5$ for 786-O and $n=4$ for WT-CLS1 spheroid cultures). * $p < 0.05$ and ** $p < 0.01$, Wilcoxon-Mann-Whitney test

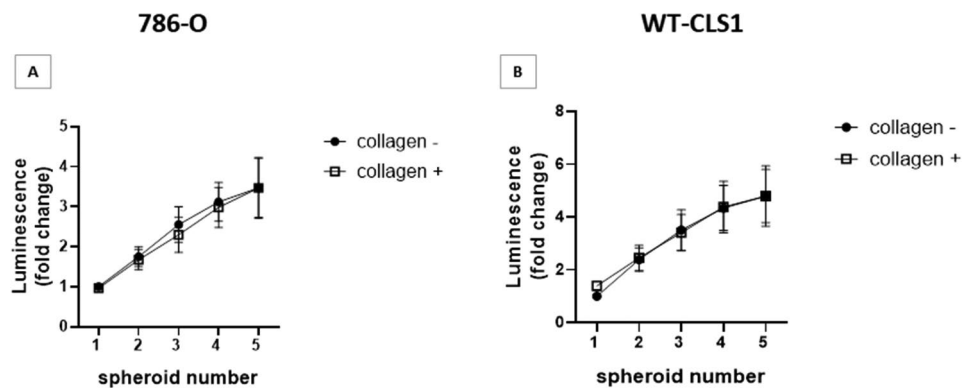


Fig. 3 Cell viability in kidney cancer spheroids treated or not with collagen I. 786-O (A) or WT-CLS1 (B) were cultured as spheroids in absence or presence of collagen I. A CellTiter-Glo 3D assay was performed on one to five cultured spheroids to measure cell viability. For each independent experiment, data are normalized to one spheroid cultured without collagen I. The figure presented is the mean \pm SEM of 3 to 4 independent experiments ($n=3$ for 786-O and $n=4$ for WT-CLS1 cells), Wilcoxon-Mann-Whitney test

Together, these results are in agreements with those obtained above.

Collagen I can interact with various receptors such as integrins and discoidin domain receptors, and it mediates intracellular signaling through AKT or ERK [4]. All the signaling assays performed so far were done with cells cultured as monolayers. To study the activation of intracellular signaling by collagen I in 3D, we stimulated the

formed spheroids as previously shown with zymogram assays. After 24-hours induction, spheroids were collected and directly lysed in Laemmli loading buffer. We analyzed the presence of active AKT (phosphorylated at Ser 473, p-AKT) depending on the spheroid number. By using either 786-O or WT-CLS1 cells, p-AKT increased rapidly, with two or three spheroids being sufficient to obtain a maximum effect on p-AKT (Fig. 5A-D).

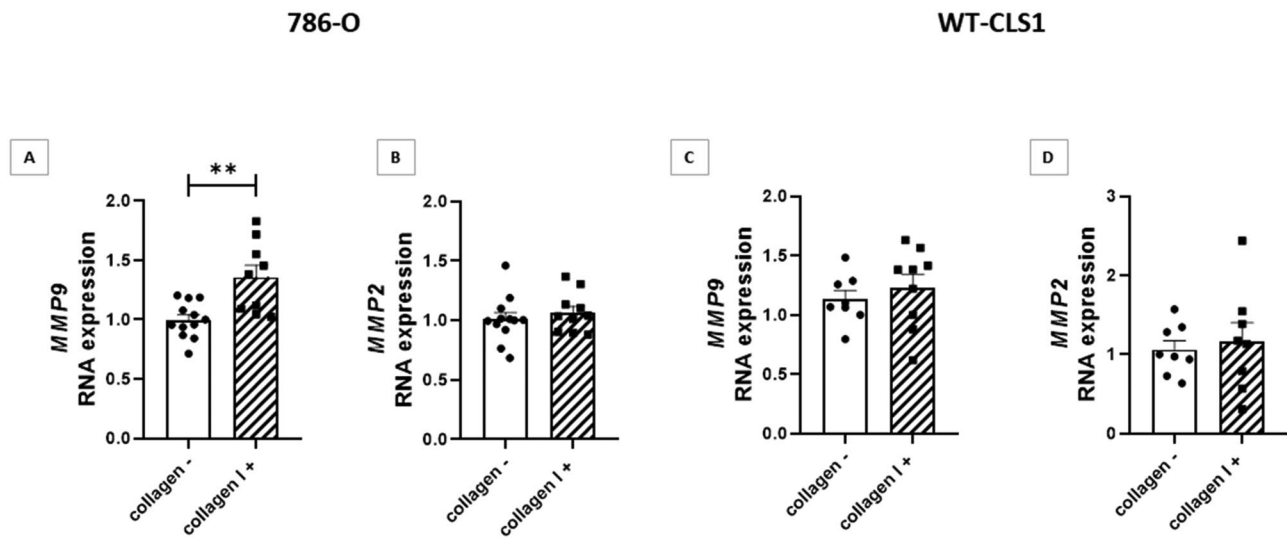


Fig. 4 Effect of collagen I on *MMP2* and *MMP9* mRNA expression in kidney cancer spheroids. Five spheroids were pooled and cultured for 24 h with or without collagen I and *MMP2* and *MMP9* mRNA levels were measured by RT-qPCR. Levels of *MMP9* transcript in 786-O (A) or WT-CLS1 (C) spheroids stimulated or not by collagen I. Levels of *MMP2* transcript in 786-O (B) or WT-CLS1 (D) spheroids stimulated or not by collagen I. For each independent experiment, the mean value of the triplicate without collagen I was used for normalization. Data are presented as the mean \pm SEM of 4 to 5 independent experiments ($n = 5$ for 786-O cells and $n = 4$ for WT-CLS1 cells). $**p < 0.01$, Wilcoxon-Mann-Whitney test

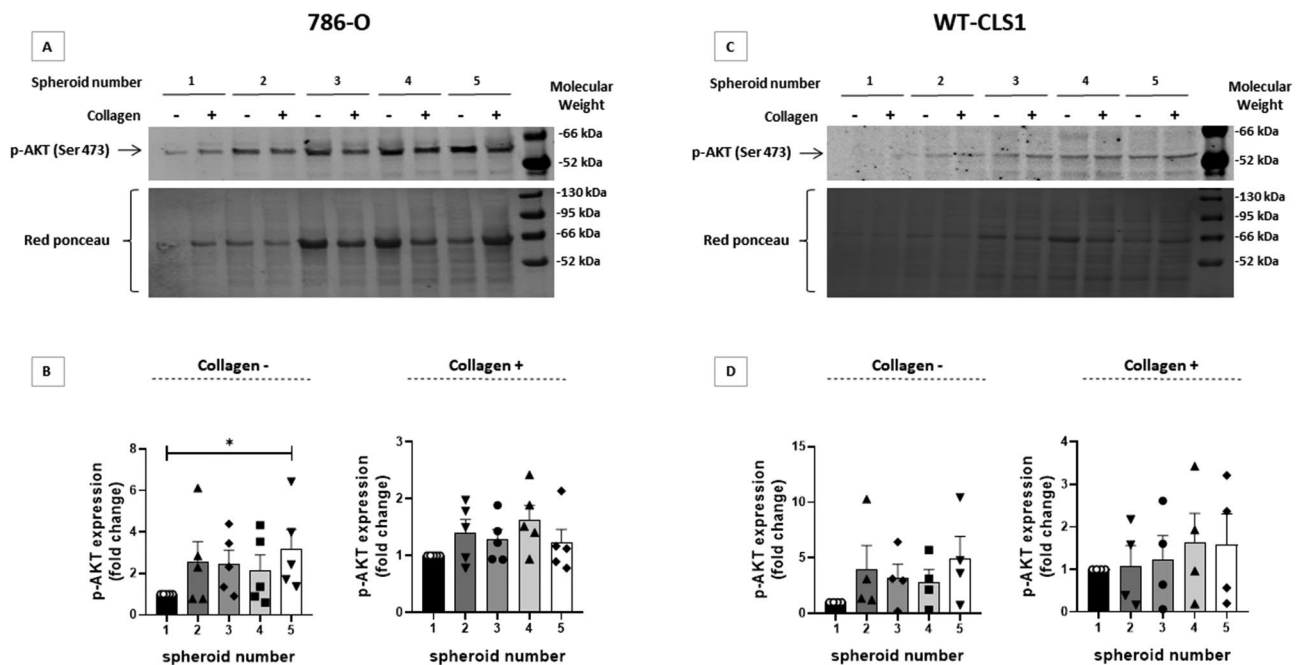


Fig. 5 Effect of kidney cancer spheroid number on AKT signaling. p-AKT (Ser 473) analysis in 786-O (A-B) or WT-CLS1 (C-D) spheroids stimulated or not with collagen I. Representative p-AKT immunoblots obtained with total protein extracts from 786-O (upper A) or WT-CLS1 (upper C) spheroids. p-AKT is shown as a 60 kDa protein. **Lower A and C**, representative Ponceau S staining of the membrane. For each independent experiment, band intensities were quantified using Fiji software (B and D) and normalized to the corresponding Ponceau S staining bands seen on the membrane. Values for a single spheroid were arbitrarily set to 1. Data are presented as the mean \pm SEM of 5 to 6 independent experiments, ($n = 6$ for 786-O and $n = 5$ for WT-CLS1 spheroid cultures), $*p < 0.05$, Kruskal-Wallis test, followed by Dunn's Multiple Comparison Test

In 786-O cells, when normalized with AKT expression, collagen I induced an inconstant phosphorylation of AKT at Ser 473 when using one to 5 spheroids in the assay. Nevertheless, with 3 spheroids, when the p-AKT

signal was at the beginning of the plateau a significant increase of p-AKT was observed under collagen I stimulation. This effect was lost with 5 spheroids (Fig. 6A). In WT-CLS1 cells, when normalized to AKT expression,

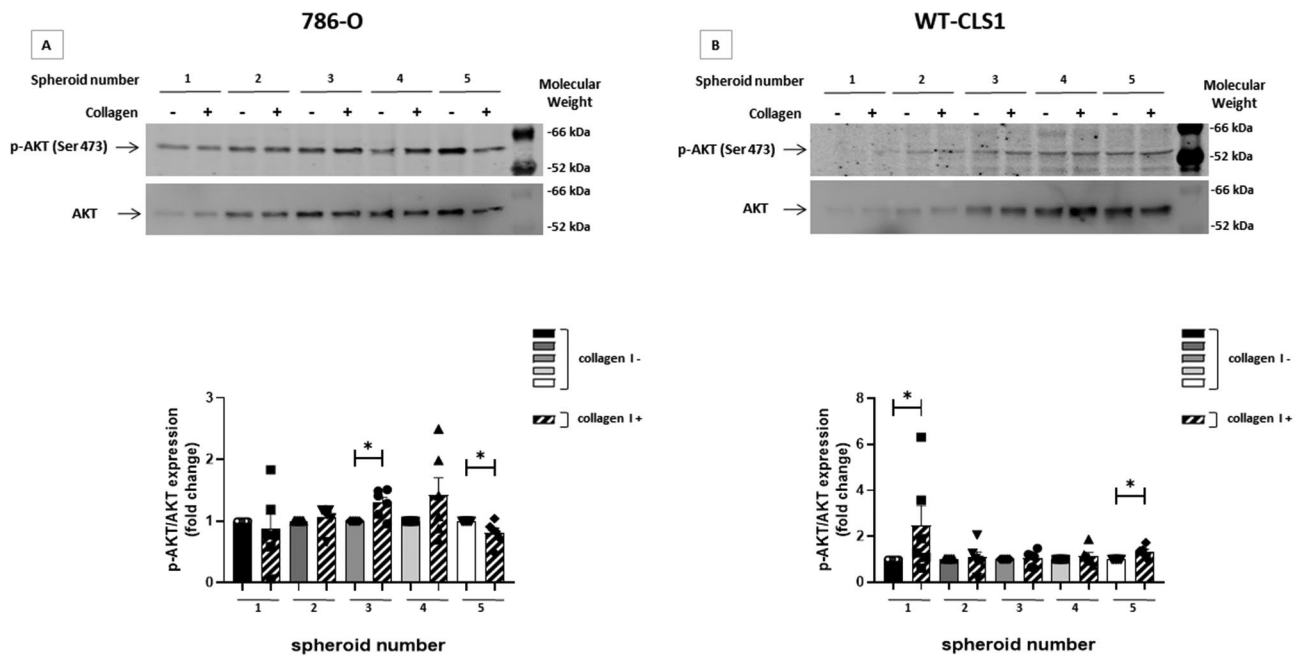


Fig. 6 Effect of collagen I on AKT pathway in kidney cancer spheroid cultures. p-AKT (Ser 473) and AKT were analyzed in 786-O (A) or WT-CLS1 (B) spheroids stimulated or not with collagen I. One to five spheroids were pooled and cultured for 24 h. p-AKT and AKT are shown as a 60 kDa protein. For each independent experiment, band intensities were quantified using Fiji software and normalized to the corresponding total AKT signal. Values without collagen I were arbitrarily set to 1. Data are presented as the mean \pm SEM of 4 independent experiments, * $p < 0.05$, Wilcoxon-Mann-Whitney test. Panel B: for one spheroid and in presence of collagen I, one outlier data point altered the mean value upwards

collagen I induced an increase in p-AKT when using one spheroid in the assay. However, when two or more spheroids were used, the effect of collagen I on p-AKT was lost (Fig. 6B).

In contrast of monolayer cell cultures, no difference in ERK activation was observed in 786-O or WT-CLS1 cells when we stimulated spheroids for short periods of time (5–90 min) with EGF (100 ng/mL), a growth factor known to activate ERK phosphorylation in ccRCC cells cultured as monolayers [13]. However, ERK activation was observed when spheroids were stimulated with a higher dose of EGF (300 ng/mL) but with different kinetics depending on the cell type and culture condition (2D *versus* 3D). In 786-O cells cultured as monolayer, EGF quickly increases ERK phosphorylation with a maximum obtained at 45 min (Fig. 7A and B). In 3D cultures, ERK phosphorylation increased rapidly, with a maximum at 15 min, and returned to basal level after 45 min of treatment (Fig. 7C and D). In WT-CLS1 cells cultured as monolayer, ERK phosphorylation increased rapidly following EGF treatment and the maximum was obtained at 15 min. At longer stimulation times ERK phosphorylation decreased but was still higher than in untreated cells (Fig. 8A and B). In 3D cultures, ERK phosphorylation increased at later time points (45 and 90 min) (Fig. 8C and D) compared to cells cultured as monolayer (15 min) suggesting a differential response of WT-CLS1 cells to EGF induction when growing in 2D *versus* 3D conditions.

Discussion

Until now, most of the zymogram assays used to measure MMP-2 and -9 activities were performed with cells growing as monolayers, but these culture conditions introduce several potential biases. In a recent work, the authors used 3D spheroid supernatants and zymogram analysis to quantify MMP-2 and -9 activities [14]. Condition media were collected and concentrated using a 10 kDa centrifugal concentrator before the zymogram assay, which increased the cost and the time to perform the experiment. To overcome these issues, we developed a rapid, cost-effective zymogram assay using cells grown as spheroids. Because one spheroid contains a limited number of cells, we pooled two to five formed spheroids in a small volume of cell medium and let them grow for an additional day in the presence or absence of collagen I. Spheroid supernatants were analyzed with a classical but optimized zymogram assay. Our data first showed that the sensitivity of the assay depends on the basal secretion of MMPs in the supernatant. If the cells secrete a large amount of MMPs, such as 786-O cells, MMP activities steadily increase with spheroid number. On the other hand, if they secrete a low amount of MMPs, as observed with WT-CLS1 cells, the MMP-2 or -9 activities increase but with lower reproducibility, likely due to the limited sensitivity of the zymogram assay and uncertainty in quantifying the different band intensities with the software (Figs. 1 and 2).

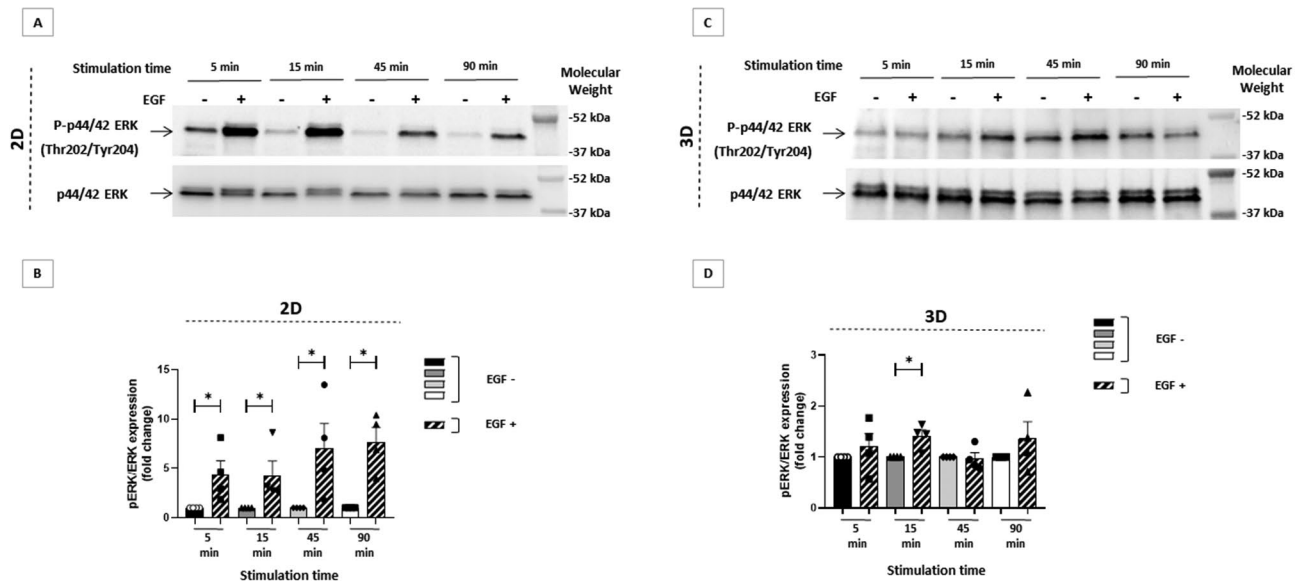


Fig. 7 Effect of EGF on ERK pathway in 786-O cells cultured as monolayer or spheroids. p-ERK or ERK were analyzed in 786-O cells cultured as monolayer (A and B) or spheroids (C and D) and stimulated or not with EGF. Five spheroids were pooled and cultured for 24 h. p-ERK and ERK are shown as 42–44 kDa proteins (A and C). For each independent experiment, band intensities were quantified using Fiji software and normalized to the corresponding total ERK signal (B and D). Values in absence of collagen I were arbitrarily set to 1. Data are presented as the mean \pm SEM of 4 to 5 independent experiments (monolayer, $n=5$; spheroids, $n=4$), * $p < 0.05$ and ** $p < 0.01$, Wilcoxon-Mann-Whitney test. P-p44/42 ERK: p-ERK, p44/42 ERK: ERK

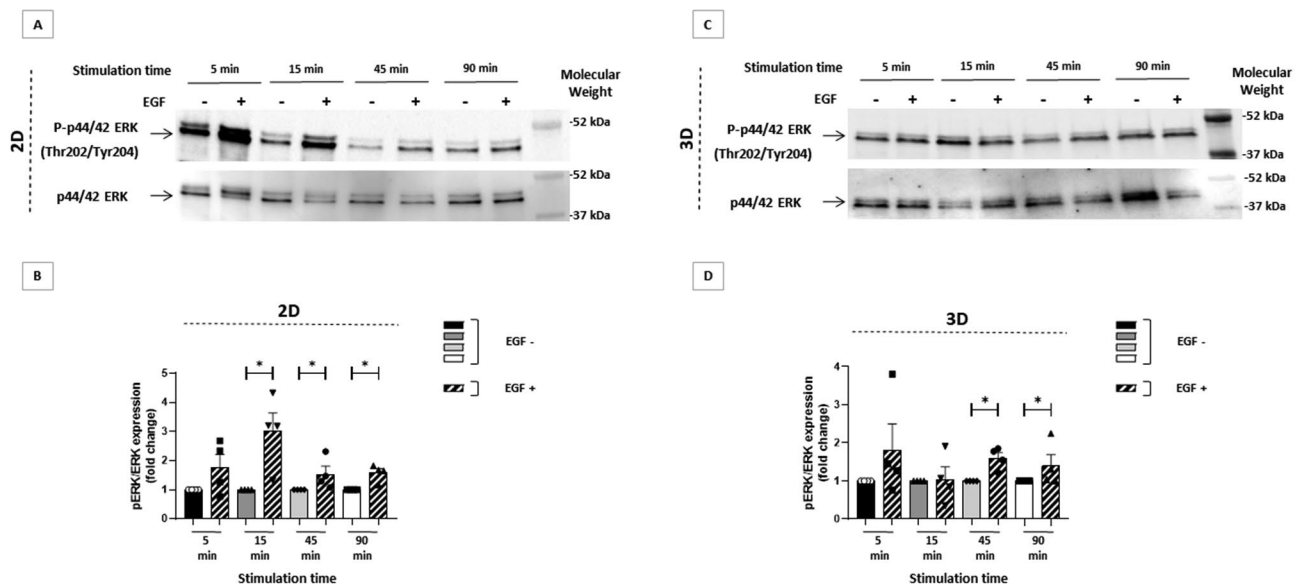


Fig. 8 Effect of EGF on ERK pathway in WT-CLS1 cells cultured as monolayer or spheroids. p-ERK and ERK were analyzed in WT-CLS1 cells cultured as monolayer (A and B) or spheroids (C and D) and stimulated or not with EGF. Five spheroids were pooled and cultured for 24 h. p-ERK and ERK are shown as 42–44 kDa proteins (A and C). For each independent experiment, band intensities were quantified using Fiji software and normalized to the corresponding total ERK signal (B and D). Values in absence of collagen I were arbitrarily set to 1. Data are presented as the mean \pm SEM of 4 independent experiments, * $p < 0.05$, Wilcoxon-Mann-Whitney test. P-p44/42 ERK: p-ERK, p44/42 ERK: ERK. Panel (B) and (D): for five spheroids and in presence of EGF for 15 (B) or 5 (D) min stimulation, one outlier data point altered the mean value upwards

In a recent study in supernatants of 786-O cells growing as monolayers and stimulated with collagen I, both MMP-9 and MMP-2 activities increased [12]. In contrast, we detected pro-MMP-9 activity but not MMP-9 activity in 786-O spheroid supernatants. Importantly, pro-MMP9

and MMP-2 activities decreased after collagen I stimulation in 786-O spheroid supernatants. This difference between 2D/3D stimulated culture has been reported in corneal fibroblasts stimulated with TGF β [15]. Compared to 2D, TGF β decreased MMP-2 activity in 3D culture,

as did collagen I in our experiments. Moreover, MMP-2 activity and expression were lower in 3D breast carcinoma or fibroblast cultures than in 2D cultures in the absence of any stimulation [14–16].

In this work, we also found that collagen I stimulation increased the abundance of *MMP9* mRNA but decreased pro-MMP-9 protein amount in supernatants. These results suggest that collagen I could induce an inhibition of *MMP9* mRNA translation and/or an inhibition in pro-MMP-9 secretion. This mechanism of translation/secretion inhibition is likely not restricted to MMP-9 since a decreased secretion of MMP-2 was found in 786-O spheroids, as for MMP-2 and MMP-9 in WT-CLS1 spheroids. However, contrarily to 786-O spheroids, collagen I did not increase *MMP9* mRNA in WT-CLS1 spheroids. This difference is likely due to the variation in the types of collagen I receptors expressed at the surface of these two cell lines. Indeed, collagen I binds different types of receptors, among which integrins and the tyrosine kinase discoidin domain receptors (DDR) [4]. As a consequence, collagen I likely induces different intracellular signaling pathways in 786-O and WT-CLS1 cells depending on its bound receptor(s) [4].

In our study, spheroids formed in the presence of collagen I secreted three-fold more pro-MMP-9 and MMP-2 than those formed in the absence of collagen I. This effect is likely due to an increase in the number of cells forming the spheroids (Supplementary Fig. 2).

After stimulating WT-CLS1 cells by collagen I, p-AKT reproducibly increased when using one spheroid, while the effect was lost with two or more spheroids. In 786-O cells the effect of collagen I on AKT phosphorylation was inconstant and related to the number of spheroids used in our experiment. As a reminder, during the 24-hours incubation period, spheroids fused to form a larger spheroid. Consequently, this fusion process might inhibit AKT activation by disturbing the formation of the hypoxic/necrotic core. Indeed, the HIF pathway activates AKT signaling in prostate cancer [17]. Alternatively, the fusion increased the expression of growth factors, such as VEGF or IGF2, which in turn could activate AKT [18]. In our 3D experiments, it is likely that the activation of AKT signaling by the HIF pathway counteracted its induction by collagen I.

The kinetics of EGF-mediated ERK activation were different in monolayer and spheroid cultures. In 2D ERK activation was quick (maximum at 45 and 15 min for 786-O and WT-CLS1 cells, respectively). In 3D the kinetic of ERK activation was biphasic with a first activation peaking at 5–15 min, followed by a decrease at 45 min and a second increase at 90 min. This biphasic kinetic may be explained by a gradient of diffusion of EGF inside the spheroid. The first peak of activation of ERK may be explained by the quick binding of EGF to its

receptor present at the surface of the cells located at the spheroid periphery. In the latter phase of induction EGF had to diffuse inside the spheroid to bind to its receptors on cells located at its center.

Compared to cells growing as monolayer which are all in contact with collagen I and the soluble growth factors (such as EGF), there is no clear information about the penetrance rate of these factors within a dense spheroid, nor the precise time to reach its center. It is also possible that only the proliferating cells which constitute the spheroid crown can respond to collagen I or EGF induction. Moreover, the same cells are likely stimulated by soluble factors produced and secreted by the cells located in the hypoxic area. Finally, the two forms of activation could function in the same direction or in totally opposite ways. Thus, additional experiments are needed to more precisely analyze the penetrance capacity of collagen I and the other soluble growth factors into the spheroids, such parameters being likely directly correlated to their size and the number of cells involved.

Conclusion and perspective

We adapted and optimized the zymogram assay to analyze MMP-2 and -9 activities in kidney cancer cells cultured as spheroids. We used collagen I, a major protein of the tumor microenvironment, to modulate MMP activities. First, we tested an increasing number of spheroids to optimize the technique and evaluate its sensitivity and reproducibility. Then, we analyzed the intracellular signals mediated by collagen I and detected inconstant activation of AKT pathway depending on the use and fusion of one to five spheroids. We successfully monitored MAPK/ERK pathway activation using 5 spheroids following cell induction with EGF. Interestingly, our data showed that the kinetic of ERK activation in spheroids is different from that observed in cells growing as a monolayer. This simple, rapid and cost-effective zymogram protocol can be adapted to any tumor cell line grown as spheroids and stimulated by collagen I or any other soluble inducer. It is also suitable for kinetic studies and time-course experiments with tumor cells grown in 3D following treatment with different growth factors or drugs.

Abbreviations

BSA	Bovine serum albumin
ccRCC	Clear cell renal cell carcinoma
ECM	Extracellular matrix
EGF	Epidermal Growth Factor
FBS	Fetal bovine serum
GPI	Glycosylphosphatidylinositol
HIF	Hypoxia-inducible factor
MMP	Matrix metalloproteinase
MW	Molecular weight
PBS	Phosphate buffer saline
RPMI	Roswell Park Memorial Institute medium
RTK	Rhabdoid tumor of the kidney

SDS PAGE	Sodium dodecyl sulfate polyacrylamide gel electrophoresis
SEM	Standard error of the mean
TBS	Tris buffer saline
TBS-T	TBS with 0.1% Tween 20
VEGF	Vascular endothelial growth factor

Supplementary Information

The online version contains supplementary material available at <https://doi.org/10.1186/s12896-025-00961-x>.

Supplementary Material 1
Supplementary Material 2
Supplementary Material 3
Supplementary Material 4
Supplementary Material 5
Supplementary Material 6
Supplementary Material 7
Supplementary Material 8
Supplementary Material 9
Supplementary Material 10
Supplementary Material 11
Supplementary Material 12

Acknowledgements

We thank all MIRCADE members for helpful discussions. The authors thank Ray Cooke for copyediting the manuscript. Bright-field and confocal microscopies were performed at the Bordeaux Imaging Center, a service unit of the CNRS-INSERM and Bordeaux University, member of the national infrastructure France BiImaging supported by the French National Research Agency (ANR-10-INBS-04).

Author contributions

P. Auguste supervised the whole study and designed the experiments with the assistance of the other authors. S. Majo, C. Redoute-Timonnier, A. Lacour, L. Challeat and E. Epinette carried out the experiments. J. Teillon made the spheroid images. S. Majo, C. Redoute-Timonnier, C. F. Grosset and P. Auguste participated in the writing, correction, and improvement of the manuscript. All authors read and approved the final version of the manuscript.

Funding

This work was supported by grants from Inserm, University of Bordeaux and from "La Ligue Contre Le Cancer, Region Aquitaine et Charentes" to Patrick Auguste. Sandra Majo received funding from "Region Nouvelle Aquitaine" (2018-1R30223) and from "Fondation Groupama, Vaincre les maladies rares, Groupama Centre Atlantique". Chloe Redoute-Timonnier is recipient of a doctoral fellowship from the "Ministère de l'Enseignement Supérieur et de la Recherche". The study was supported by donations to MIRCADE team from several charities: Aidons Marina, E.S.C.A.P.E., Eva pour la Vie, and Les Récoltes de l'Espoir.

Data availability

The datasets generated and analyzed during the current study are available from the corresponding author on reasonable request.

Declarations

Ethics approval and consent to participate

Not applicable.

Consent for publication

Not applicable.

Competing interests

The authors declare no competing interests.

Received: 19 February 2024 / Accepted: 27 March 2025

Published online: 11 April 2025

References

1. Kapałczyńska M, et al. 2D and 3D cell cultures - a comparison of different types of cancer cell cultures. *Arch Med Sci.* 2018;14:910–9.
2. Dewhurst MW, et al. Quantification of longitudinal tissue pO₂ gradients in window chamber tumours: Impact on tumour hypoxia. *Br J Cancer.* 1999;79:1717–22.
3. Lyssiotis CA, Kimmelman AC. Metabolic interactions in the tumor microenvironment. *Trends Cell Biol.* 2017;27:863–75.
4. Majo S, Auguste P. The Yin and Yang of discoidin domain receptors (DDR): Implications in tumor growth and metastasis development. *Cancers (Basel).* 2021;13:1725.
5. de Senneville BD, et al. Deciphering tumour tissue organization by 3D electron microscopy and machine learning. *Commun Biol.* 2021;4:1390.
6. Hirschhaeuser F, et al. Multicellular tumor spheroids: An underestimated tool is catching up again. *J Biotechnol.* 2010;148:3–15.
7. Molière S, Jaulin A, Tomasetto C-L, Dali-Youcef, N. Roles of matrix metalloproteinases and their natural inhibitors in metabolism: Insights into health and disease. *Int J Mol Sci.* 2023;24:10649.
8. Niland S, Riscanevo AX, Eble JA. Matrix metalloproteinases shape the tumor microenvironment in cancer progression. *Int J Mol Sci.* 2021;23:146.
9. Chhabra A, Rani V. Gel-Based gelatin zymography to examine matrix metalloproteinase activity in cell culture. *Methods Mol Biol.* 2018;1731:83–96.
10. Kotagal M, Geller J. I. Aggressive pediatric renal tumors. *Semin Pediatr Surg.* 2019;28:150860.
11. Lopez-Beltran A, et al. 2009 Update on the classification of renal epithelial tumors in adults. *Int J Urol.* 2009;16:432–43.
12. Majo S, Courtois S, Souleyreau W, Bikfalvi A, Auguste P. Impact of extracellular matrix components to renal cell carcinoma behavior. *Front Oncol.* 2020;10:625.
13. Yan Y, et al. NF-κB and EGFR participate in S1PR3-mediated human renal cell carcinomas progression. *Biochim Et Biophys Acta (BBA) - Mol Basis Disease.* 2022;1868:166401.
14. Proença S, et al. Pyridine-Containing macrocycles display MMP-2/9 inhibitory activity and distinct effects on migration and invasion of 2D and 3D breast cancer models. *Int J Mol Sci.* 2019;20:5109.
15. Umetsu A, et al. TGF-β2 induces Epithelial–Mesenchymal transitions in 2D Planar and 3D spheroids of the human corneal stroma fibroblasts in different manners. *Biomedicines.* 2023;11:2513.
16. Cardoso TC, et al. A three-dimensional cell culture system as an in vitro canine mammary carcinoma model for the expression of connective tissue modulators. *Vet Comp Oncol.* 2017;15:582–93.
17. Marhold M, et al. HIF1α regulates mTOR signaling and viability of prostate cancer stem cells. *Mol Cancer Res.* 2015;13:556–64.
18. Malekan M, Ebrahimzadeh MA, Sheida F. The role of Hypoxia-Inducible Factor-1α and its signaling in melanoma. *Biomed Pharmacother.* 2021;141:111873.

Publisher's note

Springer Nature remains neutral with regard to jurisdictional claims in published maps and institutional affiliations.